T&F-DFC FusionNet: Time&Frequency-Dynamic Functional Connectivity Fusion Network for ADHD Diagnosis in Children based on fNIRS

Mengxiang Chu[1,†], Yunxiang Ma[1,†], Xiaowei He[1], Xiao Li[1], Jiaojiao Ren[2], Zhengyu Zhong[1], Jingjing Yu[3], and Hongbo Guo[1,*]

[1] School of Information Sciences and Technology, Northwest University, Xi'an, 710127, China.
[2] Department of Pediatric Health Care, Xi'an People's Hospital (Xi'an Fourth Hospital) , Xi'an, 710004, China.
[3] School of Physics and Information Technology, Shaanxi Normal University, Xi'an, 710062, China.
[†] Co-first Author; * Corresponding Author, Guohb@nwu.edu.cn.

Abstract. Early diagnosis of attention deficit hyperactivity disorder (ADHD) in children and its underlying neurobiological mechanisms have become a focal point of research. Existing AI-based diagnostic methods show promise but struggle to fully capture dynamic correlations between brain regions, limiting their clinical effectiveness. In this study, we proposed a time&frequency-dynamic functional connectivity fusion network (T&F-DFC FusionNet) based on functional near-infrared spectroscopy (fNIRS) to assist in the objective diagnosis of children with ADHD in clinical practice. The T&F-DFC FusionNet can extract the time and frequency domain features of spatial dynamic functional connectivity across channels of fNIRS data, and improve the diagnostic results by effectively fusing multi-domain features. Meanwhile, T&F-DFC FusionNet used a leave-one-ROI-out method to study specific functional brain regions with abnormal connectivity in children with ADHD to identify clinically significant biomarkers. Through a series of experiments based on clinical data, the results show that T&F-DFC FusionNet is effective in diagnosing ADHD in children, and its performance is significantly better than that of the comparison model. In addition, notably, our findings suggest that connectivity abnormalities in the right dorsolateral prefrontal cortex and the BA 8 may be key brain regions involved in the pathogenesis of ADHD in children. In summary, this study provides new insights and methods for clinical auxiliary diagnosis and mechanism exploration of ADHD.

Keywords: children with ADHD · fNIRS · dynamic functional connectivity · time domain · frequency domain.

1 Introduction

Attention deficit hyperactivity disorder (ADHD) is a common neurodevelopmental disorder, primarily affecting children and adolescents, with potential persis-

tence into adulthood [3]. Dysregulation of brain functional connectivity (FC) plays a key role in ADHD, impacting attention, focus, and response regulation. The brain's dynamic nature, characterized by continuous reorganization of functional networks, is especially evident during cognitive tasks [11, 17]. Meanwhile, dynamic functional connectivity (DFC) is crucial for understanding the temporal dynamics and flexible reorganization of brain networks, providing insights into neural signatures linked to ADHD symptoms and cognitive deficits in children [19]. Functional near-infrared spectroscopy (fNIRS) offers a non-invasive, high-resolution method for diagnosing and studying brain function in ADHD children during cognitive tasks or clinical settings [8].

Machine learning models for fNIRS signals focus on capturing temporal dynamics from time series data for prediction. Wang et al. applied regularized linear discriminant analysis to analyze brain connectivity and distinguish ADHD individuals from healthy controls (HC) during the Stroop task [23]. For instance, Wan et al. used a multimodal EEG-fNIRS approach to explore dynamic connectivity in children with autism spectrum disorder, revealing atypical states and predicting behavioral development [19]. Tang et al. proposed a framework based on fNIRS time-domain (TD) dynamic functional connectivity to identify emotion sensitivity biomarkers, distinguishing emotional responses between nursing students and registered nurses using both unsupervised and supervised techniques [18]. While these studies highlight the effectiveness of machine learning for fNIRS data classification, traditional methods often struggle with the data's complexity due to reliance on manually extracted features and dimensionality reduction, limiting performance and increasing computational time.

Deep learning methods have emerged as more effective alternatives to address these challenges [2, 24, 16]. The TD dynamic connectivity features have been widely used for capturing important spatial relationships in functional brain networks, demonstrating their potential to enhance accuracy in brain signal classification tasks [9, 5, 13, 25]. However, a comprehensive understanding of brain signals requires both time and frequency domain (FD) considerations. Studies suggest that ADHD patients exhibit reduced dynamic variability in the time dimension, making stable connectivity patterns difficult to maintain [6, 14]. In the FD, abnormal functional activity is observed in specific frequency bands [12]. By capturing both temporal and frequency characteristics, the model extracts more comprehensive connectivity features, offering new insights and a more reliable basis for differentiating neural mechanisms between ADHD children and healthy controls.

To address the challenge that existing feature extraction methods fail to fully capture the dynamic cross-dimensional correlations between brain regions in children with ADHD, the time&frequency-dynamic functional connectivity fusion network (T&F-DFC FusionNet) based on fNIRS was proposed for objective ADHD diagnosis. By segmenting multivariate fNIRS data into time slices, T&F-DFC FusionNet could enhance the capture of multi-domain dynamic coordination between brain regions during tasks in children with ADHD by fusing TD and FD FC features in different time periods, which can improve the clinical di-

agnostic accuracy of ADHD. In addition, the T&F-DFC FusionNet model adopts leave-one-ROI-out method to evaluate the contribution of abnormal functional connectivity in different brain regions to the classification of ADHD, aiming to identify relevant biomarkers and provide region-specific evidence for clinical diagnosis.

2 Method

This section details the components of the proposed T&F-DFC FusionNet, as shown in Fig. 1(a), which includes 4 main processes. First, T&F-DFC FusionNet constructs a time domain-dynamic FC feature extraction (T-DFC) module and a frequency domain-dynamic FC feature extraction (F-DFC) module to extract the dynamic interaction patterns between brain regions in the time and frequency domains during the task process, respectively. Second, the features extracted by the T-DFC module and the F-DFC module are fused to display the FC change pattern from a multi-domain perspective and over time, and to construct the high-level spatial features of the time slice feature extraction module (Slices FEM). Third, the sampling bi-directional long short-term memory (Bi-LSTM) extracts the temporal association of the high-level spatial features of the time slice. Finally, classification is performed through two layers of dense layers.

The recorded multi-channel fNIRS data are represented as $D = \{(x_n, y_n)\}_{n=1}^{N}$, where N is the total number of samples and $x_n \in R^{t \times C}$ is the n^{th} sample containing 22 ($C_i, \quad i \in \{1, 2, \ldots, 22\}$) channels and t time points, the fNIRS sampling frames is 750. y_n is the category label of the n^{th} sample, denoted by 0 and 1 for HC and ADHD, respectively.

2.1 T-DFC feature extraction module

In the T&F-DFC FusionNet model, the T-DFC module constructs TD features through three main steps, as shown in Fig. 1(b). First, a multi-scale temporal convolutional network (MsTCN) is used to extract temporal features from each channel's time series. The MsTCN consists of three parallel temporal convolutional networks (TCN) with different kernel sizes (1×3, 1×5, 1×7), followed by a concatenation layer, enabling the capture of features at multiple time scales and improving inter-channel temporal relationship representation. This separate processing reduces noise interference and preserves channel-specific differences. The resulting channels are stacked into tensors to represent high-level temporal features. Second, temporal dynamic connectivity is analyzed by slicing each channel's time series into 10 segments, each with 75 time frames, resulting in a shape of (10, 75, 22, f_C), where 22 is the number of channels, 10 is the number of slices, 75 is the number of time frames per slice, and f_C is the number of features from the MsTCN. Finally, pearson correlation is applied to compute the FC between channels within each slice, generating a tensor T_{TS} of shape (10, 22, 22, f_C), representing the temporal DFC between channels across time and reflecting the dynamic FC changes unique to children with ADHD.

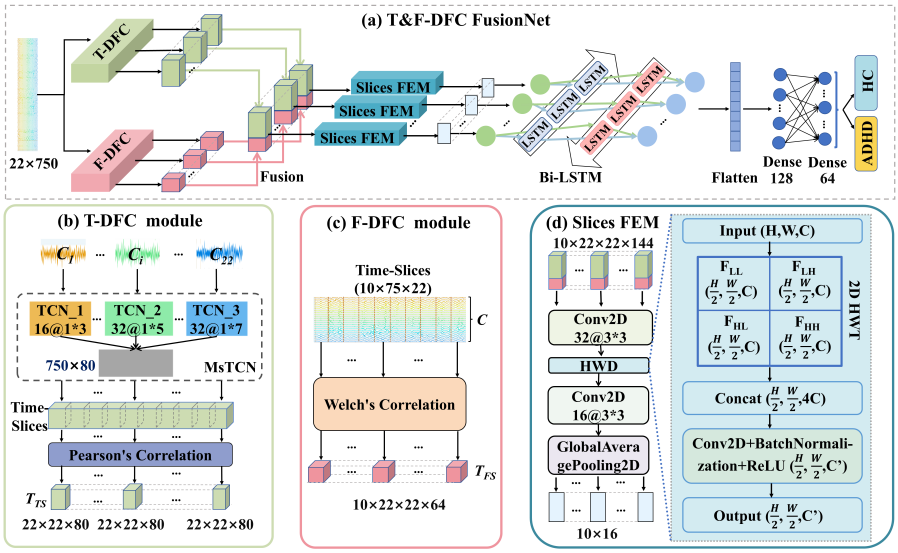

Fig. 1. The basic structure of T&F-DFC FusionNet. "a@b*c" is defined by the number of kernels, designated as "a" and the size of each kernel, represented by "b*c".

2.2 F-DFC feature extraction module

The F-DFC module analyzes functional connectivity in different frequency bands to capture neural activity differences between brain regions within specific frequency ranges, as shown in Fig. 1(c). Similar to the T-DFC module, the multi-channel time series data are sliced into segments of the same size. The coherence between channels is then computed in the FD using Welch's method [21], which calculates the power spectral density (PSD) (Eq. (1)) and cross-power spectral density (CPSD) (Eq. (2)) for each time slice [4]. The FD channel correlation, W, is derived from the PSD and CPSD, as shown in Eq. (3). This process generates an output tensor, T_{FS} with shape (10, 22, 22, f_f), where f_f is the number of frequency components, revealing the pathological differences between ADHD and HC children in specific frequency bands. In this experiment, a Hann window with a window size of 20 and an overlap rate of 50% was used to calculate W. The PSD for each channel C_i is calculated as:

$$P_{C_iC_i}(f) = \frac{1}{K}\sum_{k=1}^{K}|X_k(f)|^2, \quad i \in \{1, 2, \ldots, 22\} \tag{1}$$

where K is the number of time slices, $K = 10$. $X_k(f)$ is the spectrum obtained by applying the fast fourier transform (FFT) to the x of the k^{th} time slice. $|X_k(f)|^2$ is the normalisation factor of the windowing function. $P_{C_iC_i}(f)$ is the power spectral density of the signal under the channel C_i at frequency f. The CPSD between channels C_i and C_j is computed as:

$$P_{C_iC_j}(f) = \frac{1}{K}\sum_{k=1}^{K} X_k(f) \cdot Y_k^*(f), \quad i,j \in \{1,2,\ldots,22\} \tag{2}$$

where $Y_k^*(f)$ is the complex conjugate of the FFT of the signal from channel C_j at k^{th} time slice. $P_{C_iC_j}(f)$ is the cross-power spectral density of the signals between channels C_i and C_j. The coherence $W_{C_iC_j}(f)$ between channels C_i and C_j is derived from the PSD and CPSD as:

$$W_{C_iC_j}(f) = \frac{\left|P_{C_iC_j}(f)\right|^2}{P_{C_iC_i}(f) \cdot P_{C_jC_j}(f)}, \quad i,j \in \{1,2,\ldots,22\} \tag{3}$$

$P_{C_iC_j}(f)$ is the cross-power spectral density between channels C_i and C_j, $P_{C_iC_i}(f)$ and $P_{C_jC_j}(f)$ are the power spectral densities for channels C_i and C_j, respectively.

2.3 Feature fusion and Slices FEM

The T_{TS} and T_{FS} tensors are spliced along the time slices to align the time-frequency features, forming a fused tensor for the Slices FEM input. As shown in Fig. 1(d), each time slice of the fusion tensor is processed through a Conv2D layer, followed by Haar wavelet downsampling (HWD). The HWD structure, shown in Fig. 1(d), applies a 2D Haar wavelet transform (HWT) to decompose the input features into four frequency components: Low Frequency-Low Frequency (F_{LL}), Low Frequency-High Frequency (F_{LH}), High Frequency-Low Frequency (F_{HL}), and High Frequency-High Frequency (F_{HH}). These components are then processed through a network combining 2D sparse layers, batch normalization, and ReLU activation for non-linear enhancement [22]. Compared to traditional pooling methods, HWD preserves more local spatial information and achieves efficient feature downsampling. The downsampled tensor is passed through the next Conv2D layer for further compression and refinement of higher-order spatial features. Finally, GlobalAveragePooling2D is applied to compute the global average for each channel, resulting in more compact high-level features. The Slices FEM independently extracts high-level features from each time slice, improving the capture of dynamic functional connectivity characteristics in ADHD children.

The T&F-DFC FusionNet employs Bi-LSTM to capture dynamic time and frequency FC (128 and 64), which is then transformed into a one-dimensional vector and processed through two dense layers to realize the diagnosis of ADHD in children. The T&F-DFC FusionNet was trained with Adam (lr = 0.0001, batch size = 8), using early stopping and adaptive learning rate scheduling. Core hyperparameters were optimized through Bayesian search.

3 Experiments and Results

3.1 Data preparation and Compared methods

The 47 HC (30 males, 17 females, aged 8.62±2.41 years) and 47 ADHD children (31 males, 16 females, aged 8.79±1.98 years) were recruited from the Department of Pediatrics, Xi'an People's Hospital (Xi'an Fourth Hospital), for a verbal fluency task (VFT) experiment, which was approved by the ethics committee (approval number: KJLL-Z-H-2023005). fNIRS data were collected using the ETG-One NIRS device (Hitachi Medical, Tokyo, Japan), with oxyhemoglobin values obtained after preprocessing. Fig. 2(a) shows the spatial distribution of the 22 fNIRS channels and 6 regions of interest (ROI): left and right dorsolateral prefrontal cortex (lDLPFC, rDLPFC), medial, left and right frontal cortex (mFPC, lFPC, rFPC), and Brodmann area 8 (BA8) [10].

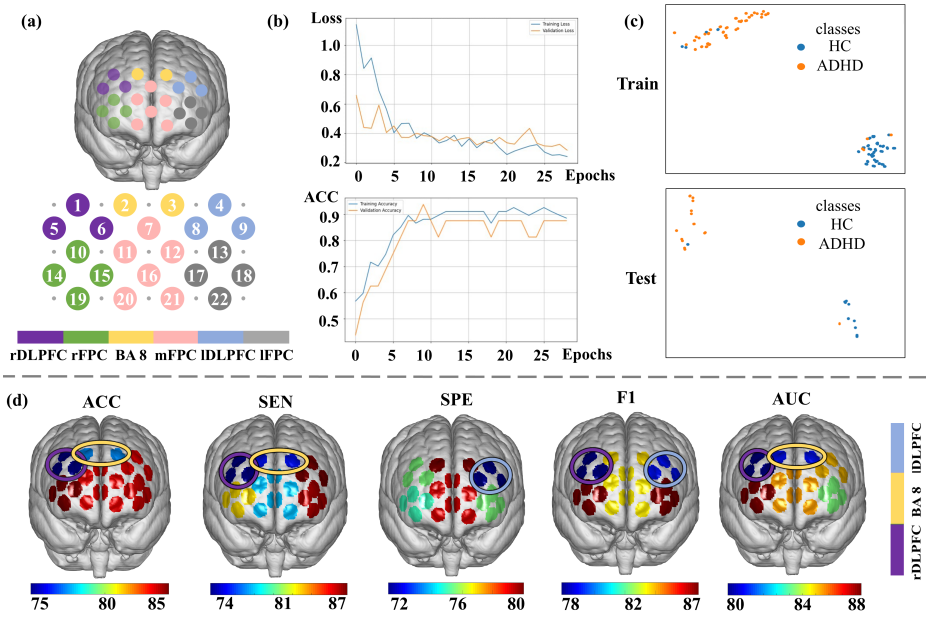

Fig. 2. (a) Spatial distribution of channels and ROIs. (b) Average loss and average ACC with 10×5-fold cross-validation. (c) t-SNE visualization of the training and test data. (d) The 3D visualization in children brain images of the performance indicators by applying the leave-one-ROI-out method, the darker the blue, the lower the performance.

Five methods were compared: two traditional classifiers, Support Vector Machine (SVM) with radial basis function kernels and Random Forest (RF) [7, 15], and three deep learning models: Transformer-T [20], ConvLSTM2D with attention mechanism (ConvLSTMwA) [1], using Pearson correlation (ConvLSTMwA-P) and Welch (ConvLSTMwA-W) for dynamic feature extraction in time and

frequency domains. All models were evaluated via five-fold cross-validation and 10 independent experiments, with 72% of data reserved for training, 8% for validation, and 20% for testing. Model performance was assessed using accuracy (ACC), sensitivity (SEN), specificity (SPE), F1-score (F1), and area under the curve (AUC).

3.2 Quantitative and Qualitative Results

Comparison with Baselines and Cluster visualization: Table 1 presents the performance of T&F-DFC FusionNet and five compared models in ADHD diagnosis. T&F-DFC FusionNet achieved an ACC of 88.25%, significantly outperforming compared models ($p < 0.05$), the SEN (94.67%), F1 (88.29%), and AUC (89.51%) were also significantly higher ($p < 0.05$), while the SPE (82.20%) was better than most compared models, though slightly lower than Transformer-T. Fig. 2(b) shows the average loss and accuracy of T&F-DFC FusionNet across 10×5-fold cross-validation, demonstrating consistent high accuracy and low loss, confirming the model's robustness and reliability in ADHD/HC classification.

Table 1. Performance comparison with baselines (Mean ± standard deviation)

Methods	ACC (%)	SEN (%)	SPE (%)	F1 (%)	AUC (%)
Ours	**88.25 (±2.47)**	**94.67 (±7.77)**	82.20 (±4.07)	**88.29 (±2.96)**	**89.51 (±5.67)**
SVM	70.40 (±9.63)	77.58 (±9.35)	54.77 (±10.73)	72.22 (±14.35)	72.44 (±15.13)
Random Forest	72.52 (±8.84)	69.90 (±12.42)	66.90 (±4.38)	71.38 (±9.19)	75.72 (±8.42)
Transformer-T	84.04 (±3.75)	80.67 (±8.48)	**85.11 (±9.48)**	82.86 (±3.75)	86.46 (±8.13)
ConvLSTMwA-P	79.71 (±9.28)	84.76 (±9.35)	74.02 (±9.74)	79.49 (±11.29)	78.51 (±9.65)
ConvLSTMwA-W	77.54 (±12.91)	76.81 (±9.93)	76.83 (±13.24)	77.46 (±12.86)	82.33 (±12.22)

Dimensionality reduction using t-SNE (complexity parameter = 30) revealed clear separation between ADHD and HC samples in both the training and test sets, as shown in Fig. 2(c). This consistent distribution supports the model's generalization ability. Additionally, t-SNE analysis demonstrated that the features extracted by T&F-DFC FusionNet preserved the dynamic properties of fNIRS signals, indicating strong discriminative power and biological relevance.

Ablation experiments: To evaluate the impact of DFC and time&frequency domain fusion feature extraction in T&F-DFC FusionNet, ablation experiments were performed. First, the T-DFC module was excluded, resulting in the construction of a frequency domain-dynamic functional connectivity network (F-DFCNet). Next, the time domain-dynamic functional connectivity network (T-DFCNet) was formed by removing the F-DFC module. Finally, time-slices were removed from both T-DFC module and F-DFC module, leading to the creation of the time&frequency-functional connectivity fusion network (T&F-FCFNet) by directly feeding the output of the Slices FEM into the fully connected layer. As shown in Table 2, removing any component decreased model performance. The absence of the single-domain DFC feature extraction module led to lower ACC, SEN, and F1 scores. Additionally, omitting dynamic synergistic features

between time slices significantly reduced ACC to 75.67%, along with substantial drops in F1 score and AUC. These results highlight the crucial role of the fusion of dynamic functional connectivity features in the time domain and frequency domain in T&F-DFC FusionNet.

Table 2. The results of ablation experiments.

Methods	ACC(%)	SEN(%)	SPE(%)	F1(%)	AUC(%)
Ours	**88.25 (±2.47)**	**94.67 (±7.77)**	**82.20 (±4.07)**	**88.29 (±2.96)**	**89.51 (±5.67)**
F-DFCNet	79.83 (±3.76)	83.39 (±15.18)	81.05 (±13.27)	79.26 (±5.42)	85.68 (±7.86)
T-DFCNet	81.01 (±13.91)	81.01 (±11.7)	82.18 (±8.89)	80.12 (±8.37)	86.59 (±7.01)
T&F-FCFNet	75.67 (±16.78)	93.81 (±5.6)	72.04 (±10.46)	79.28 (±14.16)	83.02 (±4.84)

The key biomarker assessment by leave-one-ROI-out: The leave-one-ROI-out method involved: 1) Dividing samples into five folds, using four for training and one for identifying key ROIs; 2) Training the model and saving parameters; 3) Testing the model with all ROIs for baseline performance; 4) Testing with each ROI removed by replacing channel C_i's time series with the average value; 5) Repeating for all ROIs. This process was repeated ten times to reduce randomness. Table 3 compares mean results with the baseline. Removal of the rDLPFC caused the largest drop in accuracy (-14.22%) and AUC (-11.22%), followed by BA 8 with accuracy (-11.33%) and AUC (-9.89%) drops. The Fig. 2(d) shows that the performance results of the T&F-DFC FusionNet model were presented in real children's brain images [26] after applying the leave-one-ROI-out method to control the DFC features of one ROI. The blue areas are mainly concentrated in the rDLPFC and BA8. These findings suggest rDLPFC and BA8 are crucial for ADHD classification.

Table 3. Average reduction of indicators for leave-one-ROI-out compared to baseline.

ROI-out	ΔACC%	ΔSEN%	ΔSPE%	ΔF1%	ΔAUC%
rDLPFC	**-14.22**	**-21.24**	-7.23	**-10.49**	**-11.22**
rFPC	-3.11	-12.03	-7.71	-1.42	-1.05
BA8	**-11.33**	**-19.26**	-2.16	-4.55	**-9.89**
mFPC	-4.22	-16.9	-3.85	-4.78	-4.04
lDLPFC	-4.34	-6.94	**-11.07**	**-9.23**	-4.3
lFPC	-4.02	-7.69	-7.12	-1.42	-6.17

4 Conclusion

In view of the fact that existing feature extraction methods are difficult to fully capture the dynamic correlation characteristics of different dimensions between brain regions of ADHD children, thus limiting the accuracy of clinical diagnosis,

we proposed the T&F-DFC FusionNet model for to improve clinical diagnosis. T&F-DFC FusionNet introduces the T-DFC module and F-DFC module combination layer and the Slices FEM, which can simultaneously capture the dependencies of different brain regions in the TD and FD between brain regions. The design of the model fully considers the characteristics of the continuous reorganization of brain functional connections in ADHD children when performing cognitive tasks. Through the processing of time series data slices, the establishment and extraction of brain functional connection pattern information in different dimensions, etc., the great advantages of T&F-DFC FusionNet are demonstrated. Experimental results demonstrate that T&F-DFC FusionNet outperforms traditional machine learning methods and other deep learning models, achieving high accuracy and robust performance. Additionally, the leave-one-ROI-out method identifies key brain regions, such as rDLPFC and BA8. In summary, T&F-DFC FusionNet not only enhances ADHD diagnosis in children but also provides a reliable framework for identifying biomarkers related to ADHD's underlying mechanisms, opening the door to further neuroimaging research and clinical applications.

Acknowledgments. This study was funded by: National Natural Science Foundation of China (12271434, 62271394 and 62201459); Natural Science Basic Research Program of Shaanxi Province (2023-JC-JQ-57); General Project of the Key Research and Development Plan of Shaanxi Province (2025SF-YBXM-240 and 2025SF-YBXM-380); Scientific and Technology New Star in Shaanxi Province of China (2023KJXX-035); and Research incubation project of Xi'an People's Hospital (Xi'an Fourth Hospital) (ZD-20).

Disclosure of Interests. The authors have no conflicts to disclose.

References

1. Bakhtyari, M., Mirzaei, S.: Adhd detection using dynamic connectivity patterns of eeg data and convlstm with attention framework. Biomedical Signal Processing and Control **76**, 103708 (2022)
2. Chhabra, H., Shajil, N., Venkatasubramanian, G., et al.: Investigation of deep convolutional neural network for classification of motor imagery fnirs signals for bci applications. Biomedical Signal Processing and Control **62**, 102133 (2020)
3. Coghill, D., Banaschewski, T., Cortese, S., Asherson, P., Brandeis, D., Buitelaar, J., Daley, D., Danckaerts, M., Dittmann, R.W., Doepfner, M., et al.: The management of adhd in children and adolescents: bringing evidence to the clinic: perspective from the european adhd guidelines group (eagg). European child & adolescent psychiatry pp. 1–25 (2021)
4. Damseh, R., Hireche, A., Sirpal, P., Belkacem, A.N.: Multimodal eeg-fnirs seizure pattern decoding using vision transformer. IEEE Open Journal of the Computer Society (2024)
5. Eken, A., Akaslan, D.S., Baskak, B., Münir, K.: Diagnostic classification of schizophrenia and bipolar disorder by using dynamic functional connectivity: An fnirs study. Journal of Neuroscience Methods **376**, 109596 (2022)

6. Fateh, A.A., Huang, W., Mo, T., Wang, X., Luo, Y., Yang, B., Smahi, A., Fang, D., Zhang, L., Meng, X., et al.: Abnormal insular dynamic functional connectivity and its relation to social dysfunctioning in children with attention deficit/hyperactivity disorder. Frontiers in Neuroscience **16**, 890596 (2022)
7. Fernandez Rojas, R., Huang, X., Ou, K.L.: A machine learning approach for the identification of a biomarker of human pain using fnirs. Scientific reports **9**(1), 5645 (2019)
8. Gu, Y., Miao, S., Yang, J., Li, X.: Adhd children identification with multiview feature fusion of fnirs signals. IEEE Sensors Journal **22**(13), 13536–13543 (2022)
9. He, B., Astolfi, L., Valdés-Sosa, P.A., Marinazzo, D., Palva, S.O., Bénar, C.G., Michel, C.M., Koenig, T.: Electrophysiological brain connectivity: theory and implementation. IEEE transactions on biomedical engineering **66**(7), 2115–2137 (2019)
10. Kruppa, J.A., Reindl, V., Gerloff, C., Oberwelland Weiss, E., Prinz, J., Herpertz-Dahlmann, B., Konrad, K., Schulte-Rüther, M.: Brain and motor synchrony in children and adolescents with asd—a fnirs hyperscanning study. Social Cognitive and Affective Neuroscience **16**(1-2), 103–116 (2021)
11. Li, C., Zhang, T., Li, J.: Identifying autism spectrum disorder in resting-state fnirs signals based on multiscale entropy and a two-branch deep learning network. Journal of Neuroscience Methods **383**, 109732 (2023)
12. Lin, Q., Shi, Y., Huang, H., Jiao, B., Kuang, C., Chen, J., Rao, Y., Zhu, Y., Liu, W., Huang, R., et al.: Functional brain network alterations in the co-occurrence of autism spectrum disorder and attention deficit hyperactivity disorder. European Child & Adolescent Psychiatry **33**(2), 369–380 (2024)
13. Lu, J., Zhang, X., Wang, Y., Cheng, Y., Shu, Z., Wang, J., Zhu, Z., Liu, P., Yu, Y., Wu, J., et al.: An fnirs-based dynamic functional connectivity analysis method to signify functional neurodegeneration of parkinson's disease. IEEE Transactions on Neural Systems and Rehabilitation Engineering **31**, 1199–1207 (2023)
14. Misra, R., Gandhi, T.K.: Functional connectivity dynamics show resting-state instability and rightward parietal dysfunction in adhd. In: 2023 45th Annual International Conference of the IEEE Engineering in Medicine & Biology Society (EMBC). pp. 1–4. IEEE (2023)
15. Oku, A.Y.A., Sato, J.R.: Predicting student performance using machine learning in fnirs data. Frontiers in Human Neuroscience **15**, 622224 (2021)
16. Park, J.H.: Classification of mild cognitive impairment using functional near-infrared spectroscopy-derived biomarkers with convolutional neural networks. Psychiatry Investigation **21**(3), 294 (2024)
17. Scaffei, E., Mazziotti, R., Conti, E., Costanzo, V., Calderoni, S., Stoccoro, A., Carmassi, C., Tancredi, R., Baroncelli, L., Battini, R.: A potential biomarker of brain activity in autism spectrum disorders: A pilot fnirs study in female preschoolers. Brain Sciences **13**(6), 951 (2023)
18. Tang, T.B., Chong, J.S., Kiguchi, M., Funane, T., Lu, C.K.: Detection of emotional sensitivity using fnirs based dynamic functional connectivity. IEEE Transactions on Neural Systems and Rehabilitation Engineering **29**, 894–904 (2021)
19. Wan, L., Li, Y., Zhu, G., Yang, D., Li, F., Wang, W., Chen, J., Yang, G., Li, R.: Multimodal investigation of dynamic brain network alterations in autism spectrum disorder: Linking connectivity dynamics to symptoms and developmental trajectories. NeuroImage **302**, 120895 (2024)
20. Wang, Z., Zhang, J., Zhang, X., Chen, P., Wang, B.: Transformer model for functional near-infrared spectroscopy classification. IEEE Journal of Biomedical and Health Informatics **26**(6), 2559–2569 (2022)

21. Welch, P.: The use of fast fourier transform for the estimation of power spectra: a method based on time averaging over short, modified periodograms. IEEE Transactions on audio and electroacoustics **15**(2), 70–73 (1967)
22. Xu, G., Liao, W., Zhang, X., Li, C., He, X., Wu, X.: Haar wavelet downsampling: A simple but effective downsampling module for semantic segmentation. Pattern Recognition **143**, 109819 (2023)
23. Yang, C.M., Shin, J., Kim, J.I., Lim, Y.B., Park, S.H., Kim, B.N.: Classifying children with adhd based on prefrontal functional near-infrared spectroscopy using machine learning. Clinical Psychopharmacology and Neuroscience **21**(4), 693 (2023)
24. Zhang, Y., Liu, D., Li, T., Zhang, P., Li, Z., Gao, F.: Cgan-rirn: a data-augmented deep learning approach to accurate classification of mental tasks for a fnirs-based brain-computer interface. Biomedical optics express **14**(6), 2934–2954 (2023)
25. Zhang, Y., Zhu, C.: Assessing brain networks by resting-state dynamic functional connectivity: an fnirs-eeg study. Frontiers in neuroscience **13**, 1430 (2020)
26. Zhao, T., Liao, X., Fonov, V.S., Wang, Q., Men, W., Wang, Y., Qin, S., Tan, S., Gao, J.H., Evans, A., et al.: Unbiased age-specific structural brain atlases for chinese pediatric population. Neuroimage **189**, 55–70 (2019)